JOURNAL OF CATALYSIS **163,** 279–293 (1996)
ARTICLE NO. 0329

Combustion of CO and Toluene; Characterisation of Copper Oxide Supported on Titania and Activity Comparisons with Supported Cobalt, Iron, and Manganese Oxide

Per-Olof Larsson,* Arne Andersson,*,[1] L. Reine Wallenberg,† and Bo Svensson†

*Department of Chemical Engineering II (Chemical Technology) and †Department of Inorganic Chemistry 2, University of Lund, Chemical Center, P.O. Box 124, S-221 00 Lund, Sweden

Received September 19, 1995; revised May 24, 1996; accepted June 21, 1996

Titania-supported copper oxide catalysts have been prepared with loadings in the range from $\frac{1}{3}$ to 5 theoretical layers and have been tested for the combustion of CO and toluene. Characterisation with XRD, electron microscopy, EDX, TPR, Raman, and XPS gives details about the structure of copper oxide on titania. The results show that dispersed CuO_x is formed up to a loading of about one theoretical layer. TPR indicates the formation of two types of dispersed species, which possibly are isolated and polymeric, respectively. XPS data show that the dispersed copper is Cu^{2+}. The dispersed species have high catalytic activity for combustion. At higher copper oxide loading, bulk CuO is formed, contributing little to the activity. Comparison of three titania supports with differing surface area and pore size distribution shows that the most favorable is a support with a surface area of about 38 m^2/g and mesopores in the range 100–800 Å. The longevity of the catalysts was tested in the waste gas from a formaldehyde plant. Deactivation was observed after being on stream for 57 days, and the deactivation is due to sintering of both the support and the copper oxide. Copper oxide on titania is shown to be more active than cobalt, manganese, and iron oxide on the same support.

INTRODUCTION

Volatile organic compounds (VOCs) include any organic compound found in gaseous form in the emissions from stationary, mobile, and diffuse sources. VOCs are major pollutants in the environment and are known to contribute to a number of environmental problems such as formation of ground-level ozone, formation of photochemical smog, offensive odors, and toxic air emissions. More than 70% of the air emissions are suspected to be toxic according to the U.S. Environmental Protection Agency (EPA). Although legislation has already been introduced to reduce the VOC emissions, the demands will result in more stringent and broader application of standards because of programs like the Clean Air Act Amendments in the U.S.A. The EU as well plans to legislate harder on the control of VOCs. VOC emissions often contain mixtures with numerous organic substances of variable content and are vented from mobile sources (≈40–50%) and a variety of industrial and commercial processes, e.g., printing, metal decorating, paint drying, metal degreasing, manufacturing of organic compounds and polymers, food processing, and air-stripping units (1–3).

Several end-of-pipe abatement controls are available for the reduction of VOC emissions and the most frequent in use are thermal and catalytic oxidizers, flares, condensers, and adsorbers (4). The selection of method depends on the application and is not an easy task. Catalytic incineration is a competitive abatement technique for streams with CO and/or organics, especially when the organics cannot be recycled, sold, or are present in low concentration. Compared with thermal incineration, catalytic oxidation occurs at lower temperatures and, thus, gives lower energy cost and no NO_x emission. Adsorption and condensation methods can be good options when recovery of the organics is of economic value (5, 6).

Catalytic combustion units are equipped with supported catalyst in form of either pellets or monolith. As active phase is used either precious metals, e.g., Pt and Pd, or base metal oxides, e.g., copper, chromium, and manganese oxide. The oxide catalysts are available mainly in the form of pellets or granules, while the metal catalysts can be obtained in different forms, e.g., pellets, monolith, or foam (1). Precious metals are expensive and are known to be sensitive to poisons, e.g., chlorine (5), facts that make base metal oxides an interesting alternative. However, oxides are known to be less active, less tolerant to sulphur, and sometimes less stable (7).

Many different metal oxides are known to be active for combustion of CO and VOCs, e.g., CuO, Co_3O_4, Cr_2O_3, NiO, Fe_2O_3, and MnO_2 (8, 9). The oxide can be deposited on a support to increase the dispersion and, moreover, the

[1] Correspondence to: Dr. Arne Andersson, Dept. of Chemical Engineering II, Chemical Center, P.O. Box 124, S-221 00 Lund, Sweden. Tel: +(46-46)2228280; Fax: +(46-46)149156.

0021-9517/96 $18.00

specific activity can be increased due to reaction or interaction with the support. TiO_2, which is a widely used support (10), is known in many cases to enhance the activity due to active phase-support interaction (11).

In the present work we have investigated titania as a support for copper, cobalt, iron, and manganese oxides for use in the combustion of CO and toluene in air. Copper and cobalt oxides were chosen because they are known to be active for combustion (9), while the iron and manganese oxides were tested because they give no disposal problems and have high catalytic activity. In the future, catalysts have to be prepared from materials which are harmless or can be recycled. Since the preliminary screening showed that copper oxide on titania was the best catalyst, three different supports of titania were coated with copper oxide to study the influence of pore size distribution and specific surface area. The influence of loading of copper oxide was investigated as well. Moreover, the deactivation was determined for some of the copper catalysts after 57 days on stream in a catalytic incinerator at a formaldehyde plant.

EXPERIMENTAL

Preparation of Catalysts

The catalysts were prepared by wet impregnation of commercial supports from the Norton Company. For screening of active phases, a ground titania (ISA Titania XT 25384, 150–355 μm, 48 m^2/g) was used. The support was impregnated with an appropriate amount of an aqueous solution of the metal nitrate. The nitrates used were $Cu(NO_3)_2 \cdot 3H_2O$ (Janssen Chimica, p.a.), $Co(NO_3)_2 \cdot 6H_2O$ (Janssen Chimica, p.a.), $Fe(NO_3)_3 \cdot 9H_2O$ (Janssen Chimica, p.a.) and $Mn(NO_3)_2 \cdot 4H_2O$ (Sigma Chemical Company, p.a.). The water used was deionized and the concentration of the nitrate solution was calculated from the uptake of water to give a final loading of 12 μmol active cation/m^2 surface area of the support. This loading is close to one theoretical layer of metal oxide (cf. Ref. (12)), and in the present paper this value for loading is defined as a monolayer.

For testing the influence of specific surface area and pore size on the catalytic performance, three titania supports were used in form of extrudates with a diameter of 3 mm and a length of around 6 mm. The supports were LSA Titania XT 90045 (5 m^2/g), ISA Titania XT 25384 (38 m^2/g), and HSA Titania XT 25376 (118 m^2/g), which will be referred to as TiO_2-5, TiO_2-38, and TiO_2-118, respectively, where the last number is the specific surface area in square meters per gram. The corresponding samples with a loading of one theoretical layer of copper oxide, which is not necessarily a true monolayer, are denoted $CuO_x(1)/TiO_2$-5, $CuO_x(1)/TiO_2$-38, and $CuO_x(1)/TiO_2$-118, respectively, where the figure within the parentheses is the number of CuO_x layers calculated on the basis of the surface area of the fresh support (Table 1). TiO_2-38 was also prepared with loadings of copper oxide corresponding to $\frac{1}{3}$, 2.5, and 5.0 theoretical layers (Table 1). For the highest loading, impregnation twice with intermediate drying and calcination were performed.

For all catalysts, the impregnation time was 2 h with subsequent drying for 16 h at 80°C. Finally, the catalysts were calcined at 500°C for 4 h in air, except in the case of the series that was used for screening active phases in CO oxidation, which was calcined at 400°C.

TABLE 1

Specific Surface Area, Pore Size Distribution, Pore Volume, and Water Uptake for CuO_x/TiO_2 Extrudates

Sample	Loading[a] (layers)	BET surface area[b] (m^2/g)	Pore size distribution[c] (Å)	Pore volume (cm^3/g)	Water uptake (cm^3/g)
TiO_2-118	—	118 (118)	30–400 (50, 200)	0.36	0.36
$CuO_x(1)/TiO_2$-118, fresh	1.0	56.4 (62.7)	50–500 (90, 200)	0.28	
$CuO_x(1)/TiO_2$-118, used[d]	1.0	49.8 (55.4)	60–550 (90, 200)	0.27	
TiO_2-38	—	37.7 (37.7)	100–800 (350)	0.29	0.30
$CuO_x(\frac{1}{3})/TiO_2$-38	1/3	36.7 (37.1)	100–900 (325)	0.29	
$CuO_x(1)/TiO_2$-38, fresh	1.0	33.5 (34.7)	100–800 (300)	0.28	
$CuO_x(1)/TiO_2$-38, used[d]	1.0	20.9 (21.6)	150–1200 (675)	0.25	
$CuO_x(2.5)/TiO_2$-38	2.5	29.5 (32.1)	120–900 (300)	0.25	
$CuO_x(5)/TiO_2$-38	5.0	29.1 (34.3)	120–800 (300)	0.23	
TiO_2-5	—	5.3 (5.3)	200–1700 (1000)	0.03	0.23
$CuO_x(1)/TiO_2$-5, fresh	1.0	5.4 (5.4)	400–1800 (1100)	0.04	
$CuO_x(1)/TiO_2$-5, used[d]	1.0	5.4 (5.4)	350–2500 (1100)	0.03	

[a] A theoretical monolayer is defined as 12 μmol Cu ions/m^2 surface area of support.
[b] The surface area in m^2/g of catalyst, and within brackets in m^2/g of support.
[c] The pore diameter at the distribution maximum is given within brackets.
[d] After use for 57 days in the incinerator at a formaldehyde plant.

Characterisation of Catalysts

FT-Raman spectra were recorded on a Bruker IFS 66/FRA 106 instrument, which was equipped with a low power diode pumped Nd:YAG laser and a liquid nitrogen cooled high sensitive germanium diode detector. The laser power was 100 mW, the resolution was 4 cm^{-1} and 1000 scans were recorded for every spectrum. A quartz tube, 5 mm in diameter, was used as a sample holder (180° backscattering). The catalysts were ground to particle diameters <150 μm before analysis.

X-ray diffraction (XRD) analysis of the catalysts was carried out on a Seifert XRD 3000 TT diffractometer using monochromatic Cu Kα radiation. The scanning range was 2.5°–60° (Θ) with a step size of 0.01° and a time step of 1.0 s. Compound identification was accomplished by comparison with JCPDS data (13). The measurements were made on ground samples with particle diameters <150 μm using a rotating sample holder.

The specific surface area (BET), pore volume, and pore size distribution of the samples were measured with a Micromeritics ASAP 2400 instrument using adsorption of N_2 at the temperature of liquid N_2. Pore volume and pore size distribution in the range 17–3000 Å were calculated with the method of Barrett, Joyner, and Halenda (14). All the samples were degassed at 350°C for 16 h before analysis. For comparative purposes, the pore volume was determined by twice by measuring the uptake of water during 2 h followed by drying the external surface on a piece of paper.

X-ray photoelectron (XPS) spectra were recorded on a Kratos XSAM 800 spectrometer. The recordings were performed with Mg Kα radiation (1253.6 eV). The anode was operated at an accelerating voltage of 13 kV and a current of 19 mA, and the pass energy was 80 eV at high magnification. The residual pressure inside the spectrometer was 10^{-8} torr or lower. The measurements were performed on samples which had been ground to particle diameters <150 μm and put on double-sided adhesive tape. Charging effects were corrected for by adjusting the main C 1s peak to a position of 285.0 eV. Due to photoreduction of dispersed copper oxide being observed to occur in the spectrometer, the data reported are for single scan spectra. For quantitative purposes instrumental sensitivity factors, 1.8 for Ti 2p and 6.3 for Cu 2p, were used, together with linear baselines.

Temperature-programmed reduction (TPR) profiles were recorded on a Micromeritics TPD/TPR 2900 instrument. The temperature was increased from 30°C to 1000°C with a heating rate of 10°C/min, and the reduction gas with a flow rate of 50 ml/min was 5 vol% H_2 in N_2. The produced water was condensed in a cold trap at about −90°C. The reactor was a quartz tube with a diameter of 4 mm. The amount of sample was 0.142 g with particle sizes in the range 150–355 μm.

Energy dispersive X-ray analysis (EDX), point analysis, and mapping of elements, was performed with a Link AN 10000 system attached to a JEOL JSM 840A scanning electron microscope. The catalyst pellets were cut along the long axis, as well as perpendicularly to it. For transmission electron microscopy (TEM), a JEOL JEM 2000FX microscope was used with a Link AN 10000 system attached for EDX point analysis and quantification.

Testing of Catalysts

The catalytic tests were performed using an adiabatic reactor made of stainless steel and with an internal diameter of 21 mm. The reactor was surrounded with an insulation section, containing a temperature-controlled heat barrier to create close to ideal adiabatic conditions. The inlet flows of N_2, O_2, and CO were fed to a mixing unit from mass flow controllers. A stream with toluene was obtained by bubbling N_2 through a temperature-controlled evaporator containing liquid toluene. Before reaching the adiabatic reactor, the gas mixture was passed through a preheater. The feed temperature was increased linearly at 2°C/min with simultaneous product analysis. Experiments were performed with either constant surface area of catalyst in the reactor or at constant GHSV (gas hourly space velocity). GHSV is defined as the total flow rate of gas at STP per unit volume of catalyst. The feed concentration of CO was 1.0 vol% in synthetic air, and the corresponding concentration of toluene was either 250 or 1000 ppm, as indicated in the text.

CO and CO_2 were analyzed with an IR instrument (Fuji electronic ZRF IR-analyser), and toluene was analysed with a flame ionisation detector (Signal 3001). Both of the instruments allowed continuous recording of the concentration. A GC Varian 3400 equipped with an FID detector and a 3 m × $\frac{1}{8}$ inch column, containing Chromosorb W, 80–100 mesh, with 20 wt% SE-30, was operated at 80°C to analyse for by-products. The temperatures before and after the reactor were measured and recorded on a PC, together with the concentrations of CO and CO_2 from the IR instrument and the concentration of hydrocarbon from the flame ionization detector. All conversions were calculated on the basis of the CO and toluene concentrations.

The catalysts in form of extrudates were aged for 57 days in the catalytic incinerator of a formaldehyde plant at Perstorp AB. Presently, the incinerator contains a Pt/Al_2O_3 catalyst and is working adiabatically at about 480°C with the inlet temperature around 280°C. The waste gas stream to the incinerator contains CO (0.8–2.0 vol%), H_2O (3 vol%), methanol (1000–1500 ppm), dimethylether (3000–5000 ppm), formaldehyde (100–500 ppm), O_2 (7 vol%), and N_2 as balance. The oxide catalysts were placed in tubes of stainless steel and were inserted in the Pt/Al_2O_3 bed. After 57 days, the oxide catalysts were tested for CO oxidation using the same method as was used to test the fresh samples, thus giving a measure of the deactivation.

RESULTS

Catalytic Tests

Comparison of different active phases for the combustion of CO and toluene. Figure 1 shows that the best active phase on TiO_2 (anatase, 48 m^2/g) in terms of specific activity for complete oxidation of 1.0 vol% CO in air is CuO_x, which is followed by CoO_x, MnO_x, and finally FeO_x. Also for combustion of 1000 ppm toluene in air CuO_x is the most active phase on TiO_2 (Fig. 2), but in this case CoO_x is the least active phase. FeO_x and MnO_x have similar activity, but they are considerably less active than CuO_x, although better than CoO_x.

Figures 1 and 2 show typical S-shape dependences for the conversion as a function of the inlet temperature to the adiabatic reactor. The steep rise in conversion, especially in the case of toluene combustion, is due to the heat produced per unit time in the reaction exceeding that which is going out with the outlet stream. A thorough theoretical analysis of the adiabatic reactor has been given by Froment and Bischoff (15). It is worthy of note that in applications there is no reason to operate a catalytic incinerator under isothermal conditions. Instead, adiabatic operation is preferred, where the temperature of the outlet stream preferably should be high enough to preheat the inlet stream to the ignition temperature, i.e., autothermic operation.

Complete oxidation of CO on CuO_x/TiO_2 extrudates. Considering Fig. 3, the best catalyst at constant GHSV using the different supports of TiO_2 with 12 μmol Cu/m^2 surface area of support is the $CuO_x(1)/TiO_2$-38 preparation followed by the $CuO_x(1)/TiO_2$-118 sample, which needs about 30°C higher inlet temperature for the same conversion. The $CuO_x(1)/TiO_2$-5 catalyst is less active and compared with $CuO_x(1)/TiO_2$-118, it requires about 40–50°C higher temperature for a given conversion.

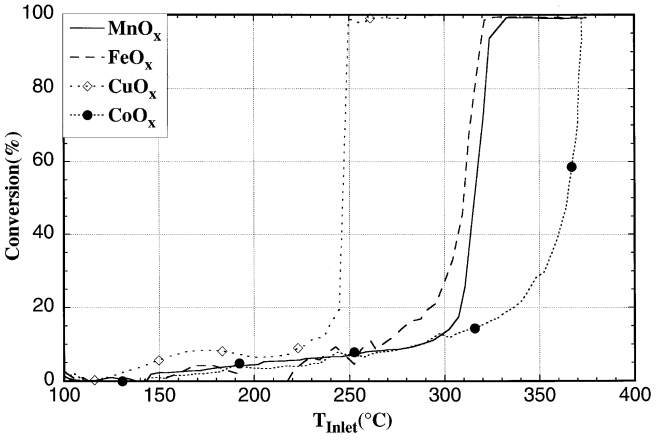

FIG. 2. Comparison of different active phases on TiO_2 (anatase, 48 m^2/g) for the combustion of 1000 ppm toluene in air. Loading of active phase: 12 μmol cation/m^2 surface area of support; particle size: 150–355 μm; total surface area in catalyst bed: 1063 m^2; GHSV: 33,500–36,500 h^{-1}; and total feed rate: 14.5 liters/min.

When increasing the loading of CuO_x on TiO_2-38 to 2.5 and 5.0 theoretical layers, the performance does not improve (Fig. 4). Compared with the monolayer sample, the conversions are about the same at the different temperatures. If the loading of CuO_x, on the other hand, is reduced to $\frac{1}{3}$ of a monolayer, the activity becomes lower. The inlet temperature has to be increased by 30–40°C for obtaining a conversion which is comparable with those shown by the samples with higher loading.

The best catalyst for the complete oxidation of 1.0 vol% CO in air, $CuO_x(1)/TiO_2$-38, was compared with two commercial catalysts, one Pt/Al_2O_3 and one metal oxide catalyst

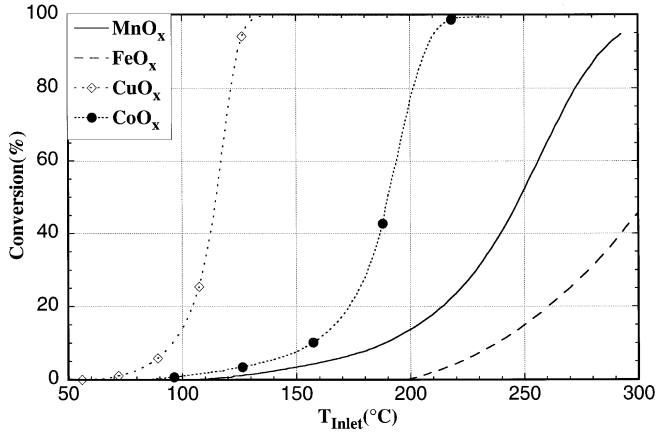

FIG. 1. Comparison of different active phases on TiO_2 (anatase, 48 m^2/g) for the oxidation of 1.0 vol% CO in air. Loading of active phase: 12 μmol cation/m^2 surface area of support; particle size: 150–355 μm; total surface area in catalyst bed: 1063 m^2; GHSV: 33,500–36,500 h^{-1}; and total feed rate: 14.5 liters/min.

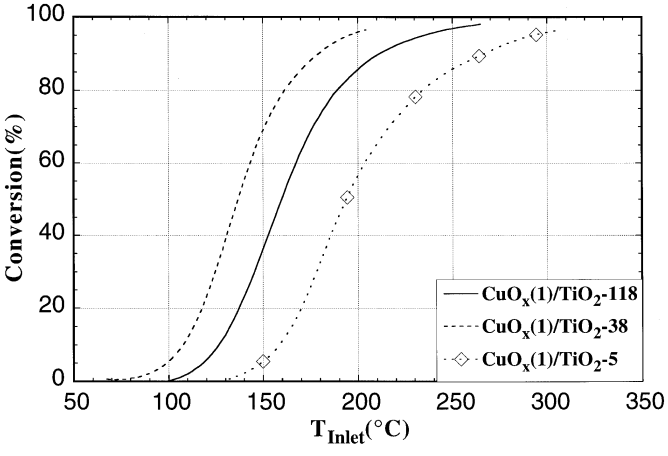

FIG. 3. Comparison of CuO_x on different TiO_2 supports for the oxidation of 1.0 vol% CO in air. Loading of active phase: 12 μmol Cu/m^2 surface area of support; particle size: extrudates 3 mm (diameter) × 6 mm (length); GHSV: 20,000 h^{-1}; and total feed rate: 8.65 liters/min.

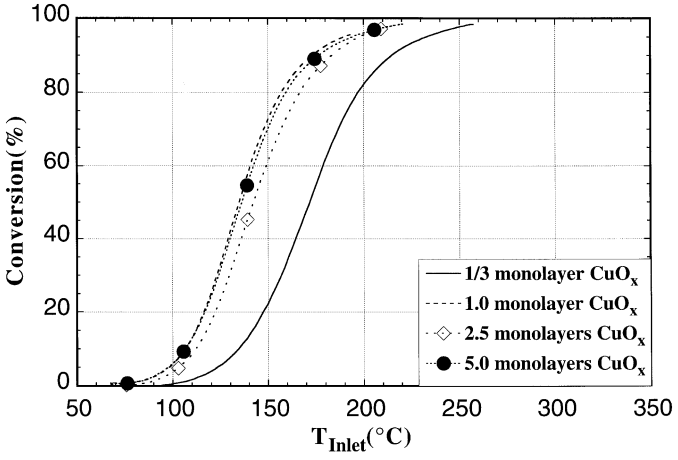

FIG. 4. Influence of loading of CuO_x on TiO_2-38 for the oxidation of 1.0 vol% CO in air. Particle size: extrudates 3 mm (diameter) × 6 mm (length); GHSV: 20,000 h^{-1}; and total feed rate: 8.65 liters/min.

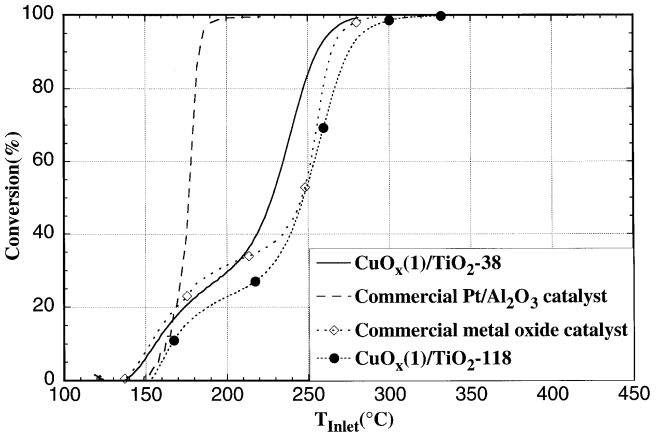

FIG. 6. Conversion of 250 ppm toluene in air. Comparison of the performances of CuO_x on two titania supports with monolayer loading, a commercial Pt/Al_2O_3 catalyst, and a commercial base metal oxide catalyst. GHSV: 20,000 h^{-1}; and total feed rate: 8.65 liters/min.

(Fig. 5). The $CuO_x(1)/TiO_2$-38 catalyst is more active than the commercial base-metal oxide catalyst and at low conversion also more active than the Pt/Al_2O_3 catalyst. However, at high conversion Pt/Al_2O_3 is the best, followed by the $CuO_x(1)/TiO_2$-38 catalyst.

Combustion of toluene on CuO_x/TiO_2 extrudates. The $CuO_x(1)/TiO_2$-38 and $CuO_x(1)/TiO_2$-118 catalysts were tested for the combustion of 250 ppm toluene in air (Fig. 6). The $CuO_x(1)/TiO_2$-38 catalyst is the most active of the two and requires about 20°C less temperature than $CuO_x(1)/TiO_2$-118 for the same conversion level.

$CuO_x(1)/TiO_2$-38 was also compared with the same two commercial catalysts which were tested for the oxidation of CO (Fig. 6). In this case, the Pt/Al_2O_3 catalyst is the most active and requires 80°C less inlet temperature than $CuO_x(1)/TiO_2$-38 for giving the same conversion level. The $CuO_x(1)/TiO_2$-38 catalyst is just slightly more active than the commercial oxide catalyst.

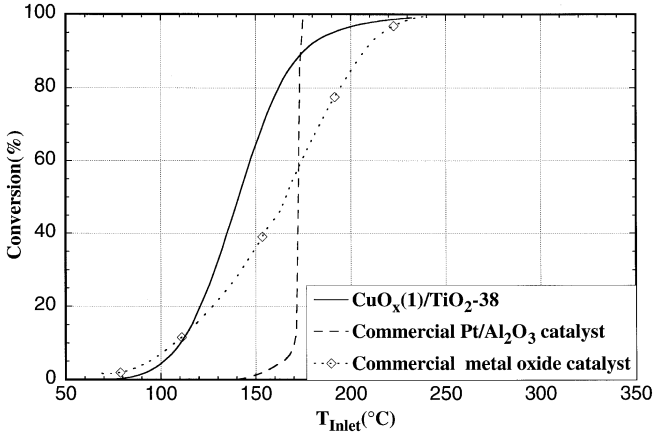

FIG. 5. Comparison of the monolayer $CuO_x(1)/TiO_2$-38 catalyst with a commercial Pt/Al_2O_3 catalyst and a commercial base metal oxide catalyst for the oxidation of 1.0 vol% CO in air. GHSV: 20,000 h^{-1}; and total feed rate: 8.65 liters/min.

Deactivation test. After being on stream for 57 days in a catalytic incinerator at a formaldehyde plant, the catalysts with monolayer loading of CuO_x on the different TiO_2 supports were retested for the combustion of 1.0 vol% CO in air under the same experimental conditions which were used to test the samples in fresh form. The $CuO_x(1)/TiO_2$-38 catalyst shows small deactivation (Fig. 7b), 20°C at most for low conversions and at high conversions there was no visible deactivation. Moreover, the sample deactivates little as compared to $CuO_x(1)/TiO_2$-118 (Fig. 7a) and $CuO_x(1)/TiO_2$-5 (Fig. 7c).

Specific Surface Area, Pore Size Distribution, and Pore Volume

The results of the volumetric measurements are collected in Table 1. The TiO_2-118 support has a specific surface area of 118 m^2/g and the pore volume, according to the BJH method (14), is 0.36 cm^3/g. The latter value is equal to the measured uptake of water. The pore size distribution is bimodal in the range 30–400 Å with maxima at 50 and 200 Å. After deposition of monolayer loading on TiO_2-118 with copper and following calcination, the specific surface area and the pore volume have decreased to 56.4 m^2/g and 0.28 cm^3/g, respectively. The pore sizes are between 50 and 500 Å with a maximum at 200 Å and a second small maximum at 90 Å. For the used $CuO_x(1)/TiO_2$-118 catalyst the specific surface area is 49.8 m^2/g, the pore volume is 0.27 cm^3/g and the pore size distribution, likewise, has not changed much.

The TiO_2-38 support has a specific surface area of 37.7 m^2/g, a pore volume of 0.29 cm^3/g and the uptake of water is 0.30 cm^3/g. The pore size distribution is rather broad,

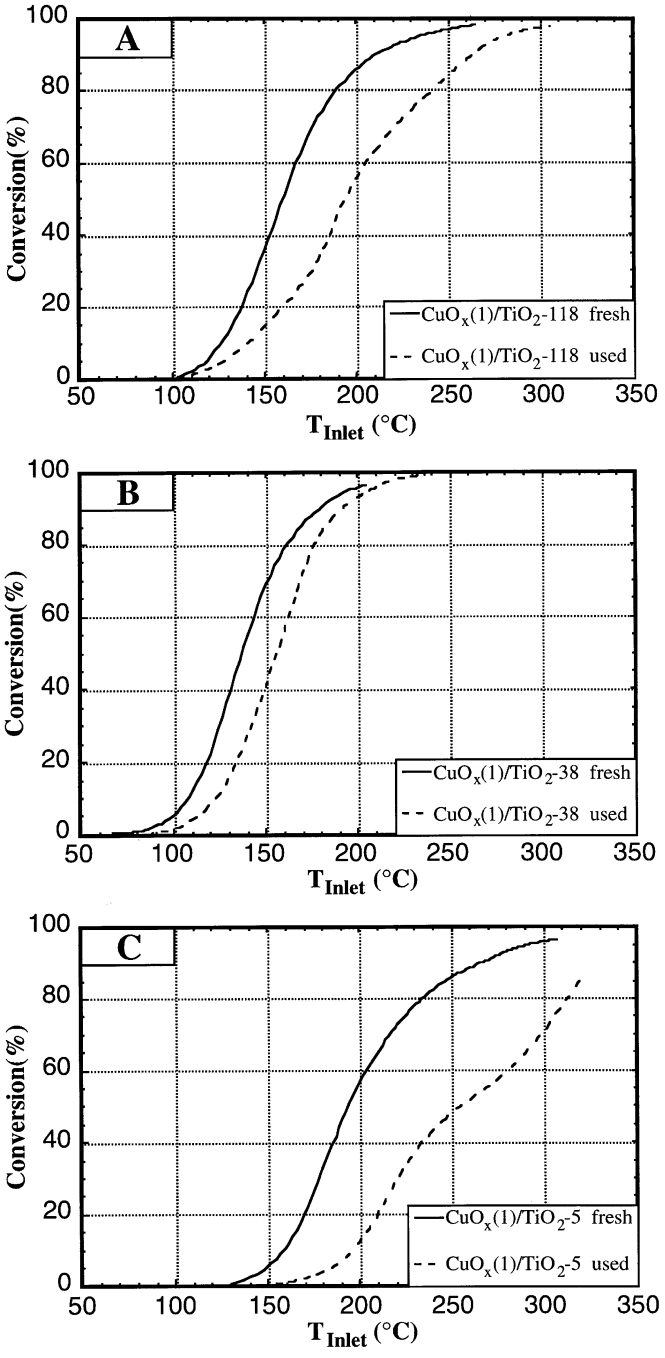

FIG. 7. The conversion of 1.0 vol% CO in air as a measure of the deactivation of monolayer CuO_x/TiO_2 catalysts after being on stream for 57 days in an incinerator at a formaldehyde plant: (A) $CuO_x(1)/TiO_2$-118; (B) $CuO_x(1)/TiO_2$-38; and (C) $CuO_x(1)/TiO_2$-5. Particle size: extrudates 3 mm (diameter) × 6 mm (length); GHSV: 20,000 h^{-1}; and total feed rate: 8.65 liters/min.

100–800 Å, with a maximum at 350 Å. With increase in loading of CuO_x the pore size distribution is hardly affected, while the specific surface area and the pore volume both decrease slightly. This is partly due to decrease of the molar fraction of support. After being on stream for 57 days, the specific surface area of the $CuO_x(1)/TiO_2$-38 catalyst has decreased to 20.9 m^2/g and the pore volume to 0.25 cm^3/g. Simultaneously, the pore size distribution has changed to the interval 150–1200 Å with a maximum at 675 Å.

The TiO_2-5 support has a specific surface area of 5.3 m^2/g. In this case, the pore volume value (0.03 cm^3/g) does not agree with the uptake of water (0.23 cm^3/g). The latter value is higher, possibly due to the presence of macropores. Deposition of a theoretical monolayer of CuO_x on the TiO_2-5 support does not affect the specific surface area or the pore volume, but blocks some of the smallest pores. The mesopore sizes of the fresh $CuO_x(1)/TiO_2$-5 are between 400 and 1800 Å, with a maximum at 1100 Å. Use of the sample for 57 days does not lead to any significant change in the specific surface area or the pore volume, but the pore size distribution has extended to 350–2500 Å, although with the same maximum at 1100 Å as for the fresh catalyst.

X-Ray Diffraction

Table 2 shows some characteristic XRD data for the extrudates. The TiO_2-118 sample was nearly X-ray amorphous and showed broad XRD lines. Both TiO_2-118 and TiO_2-38 consist of pure anatase (JCPDS file no. 21-1272) with no rutile (JCPDS file no. 21-1276) because no peak is apparent at $\Theta = 13.7°$, where the strongest line from rutile is positioned (13). TiO_2-5, on the other hand, consists of both anatase and some rutile. The intensity ratio between the strongest line of rutile ($\Theta = 13.7°$) to that of anatase ($\Theta = 12.7°$) is 5.3%, corresponding to about 6.3% of rutile following the formula given by Spurr and Myers (16). Generally, the data in Table 2 show a relationship between the full width at half maximum (FWHM) for anatase and the specific surface area (Table 1) and, in fact, the crystallite size.

For the $CuO_x(1)/TiO_2$-118 sample, CuO lines (JCPDS file no. 41-254) (13) appear, of which two strong lines are at $\Theta = 17.8°$ and $\Theta = 19.4°$. The formation of CuO can be understood considering the loss of surface area which occurs upon deposition of copper and subsequent calcination (Table 1). Upon use of the catalyst, the crystallinity of the support increases as is seen from the narrowing of the FWHM of the strongest anatase peak.

In case of the TiO_2-38 support with various copper loadings, the CuO line at $\Theta = 17.8°$ is detected from 2.5 theoretical layers and above. The CuO line at $\Theta = 19.4°$ unfortunately interferes with a peak from anatase at $\Theta = 19.2°$ (13). However, compared with the pure support, the peak at $\Theta = 19.3$–$19.4°$ is more intense at all loadings of copper oxide ($\frac{1}{3}$ to 5.0 layers). The only difference between the fresh and the used $CuO(1)/TiO_2$-38 catalyst is the decrease of the FWHM for the anatase peak, corresponding to crystal enlargement.

No peaks except those shown by the TiO_2-5 support are seen in the pattern for $CuO_x(1)/TiO_2$-5. Apparently, this is due to the absolute amount of active phase being small

TABLE 2

Some Characteristic X-ray Diffraction Peaks for CuO_x/TiO_2 Catalysts and Supports

Sample	Anatase (1 0 1)		Rutile (1 1 0)		CuO (−1 1 1)		Anatase (1 1 2); CuO (2 0 0)	
	Θ (°)	FWHM[a] (°)	Θ (°)	$I/I_O \cdot 100$[b]	Θ (°)	$I/I_O \cdot 100$[b]	Θ (°)	$I/I_O \cdot 100$[b]
TiO_2-118	12.68	0.26	—	—	—	0	—	—
$CuO_x(1)/TiO_2$-118, fresh	12.68	0.19	—	—	17.81	9.8	19.37	15.7
$CuO_x(1)/TiO_2$-118, used[c]	12.69	0.17	—	—	17.81	8.1	19.31	14.6
TiO_2-38	12.69	0.13	—	—	—	0	19.32	7.9
$CuO_x(\frac{1}{3})/TiO_2$-38	12.69	0.14	—	—	—	0	19.29	9.6
$CuO_x(1)/TiO_2$-38, fresh	12.68	0.14	—	—	—	0	19.32	10.0
$CuO_x(1)/TiO_2$-38, used[c]	12.69	0.12	—	—	—	0	19.30	9.6
$CuO_x(2.5)/TiO_2$-38	12.68	0.13	—	—	17.75	4.7	19.34	13.0
$CuO_x(5)/TiO_2$-38	12.68	0.13	—	—	17.79	14.0	19.37	19.4
TiO_2-5	12.69	0.07	13.76	5.3	—	0	19.32	8.9
$CuO_x(1)/TiO_2$-5, fresh	12.68	0.07	13.75	5.6	—	0	19.31	8.1
$CuO_x(1)/TiO_2$-5, used[c]	12.69	0.06	13.75	8.5	—	0	19.32	7.9

[a] FWHM: full width at half maximum.
[b] I/I_O: Ratio of the peak intensity to that for the (1 0 1) anatase line.
[c] After use for 57 days in the incinerator at a formaldehyde plant.

and well dispersed. The fresh $CuO_x(1)/TiO_2$-5 has about the same proportion of rutile as the pure support. However, upon use the catalyst, the proportion of rutile increases about 50%. The FWHM for the anatase line at $\Theta = 12.7°$ remains unchanged.

Temperature Programmed Reduction

TPR profiles for TiO_2-38 with different loadings of copper oxide are shown in Fig. 8. For the samples with 1.0, 2.5, and 5.0 theoretical layers of CuO_x, one peak of equal size appears around 180°C and there is a second peak at 230–280°C, which grows in amplitude when the loading increases. For the latter peak the temperature at the peak maximum increases with increased loading. The TPR profile for $CuO_x(\frac{1}{3})/TiO_2$-38 shows one peak at about 200°C and another weak peak at 250°C. The peak at 200°C is seen as well as a shoulder in the curve for $CuO_x(1)/TiO_2$-38. Moreover, for all loadings there is a broad peak of equal size at 420°C. The TPR curve of pure CuO showed reduction in a single peak with rate maximum at 340°C, while the pure TiO_2-38 support gave a peak at 650°C.

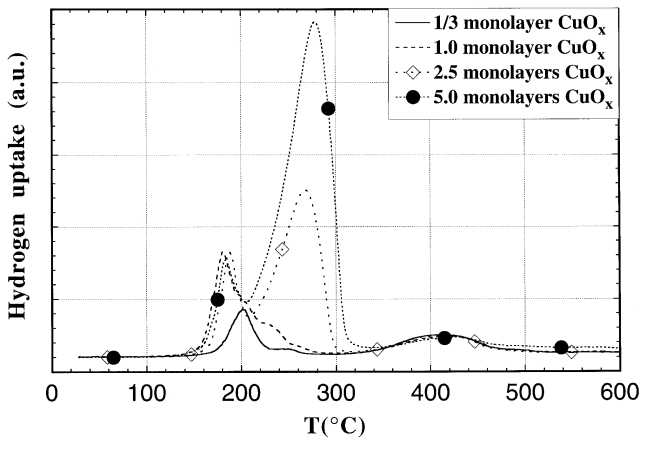

FIG. 8. TPR profiles for different loadings of CuO_x on TiO_2-38. Sample size: 0.142 g.

Freshly prepared $CuO_x(1)/TiO_2$-118 has peaks at 200, 250, and 390°C (Fig. 9a). After use of the sample the first peak has diminished, the second one has become broader, and the third remains unchanged. The features of the TPR curve of the used $CuO_x(1)/TiO_2$-38 catalyst (Fig. 9b) indicate some sintering of dispersed copper oxide because, compared with the spectrum of the fresh sample, the peak at 180°C is smaller while the peak at 250°C is larger and has shifted from 230°C. The peak around 400°C has decreased somewhat in amplitude. $CuO_x(1)/TiO_2$-5 in fresh form shows only the peaks at 180°C and 230°C (Fig. 9c). In this case, there is no peak around 400°C, which appears using the titania supports with higher specific surface area (Figs. 9a and 9b). The curve for the used $CuO_x(1)/TiO_2$-5 shows the almost complete absence of the peak at 180°C and the appearance of a new peak at 270°C.

X-Ray Photoelectron Spectroscopy

The binding energies, half widths, Cu/Ti surface ratio and the intensity ratio between the Cu $2p_{3/2}$ shake-up satellite and the main peak are summarized in Table 3 for CuO_x/TiO_2 catalysts, supports, and CuO. The Cu $2p_{3/2}$ binding energy for the pure CuO is 934.3 eV and is about the same for the copper oxide supported on TiO_2, both before and after use in the incinerator. The Ti $2p_{3/2}$ binding energy is at

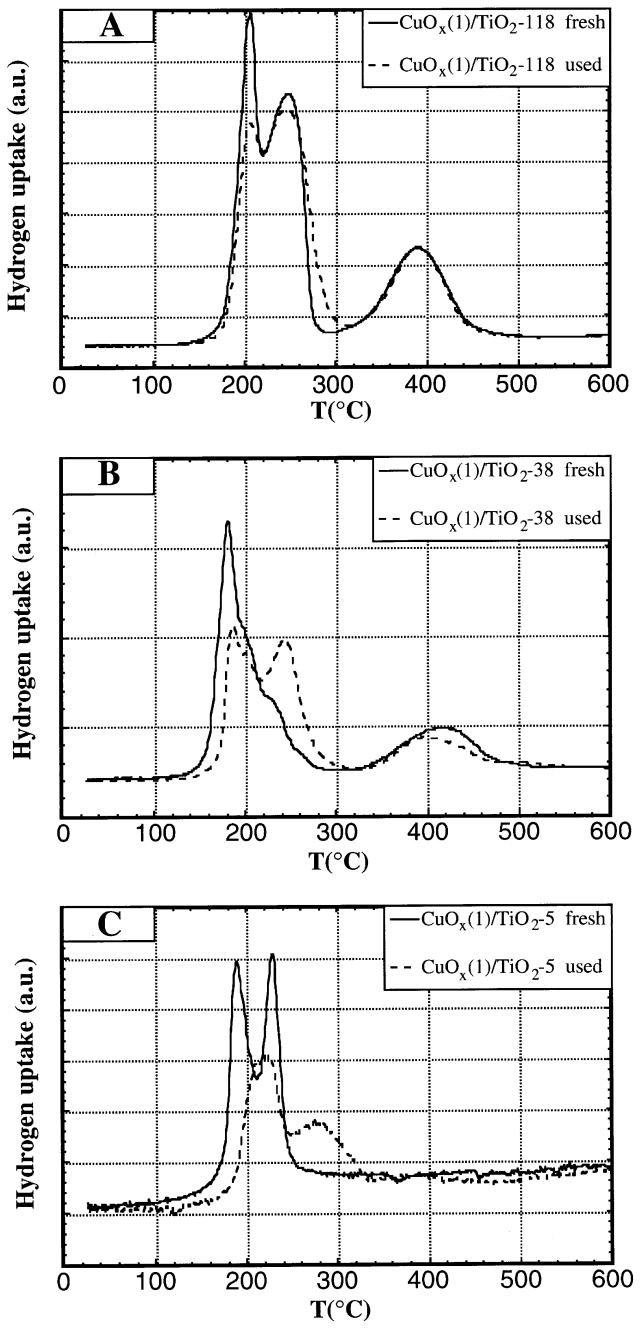

FIG. 9. Normalised TPR profiles for monolayer CuO_x/TiO_2 catalysts before and after use in an incinerator for 57 days: (A) $CuO_x(1)/TiO_2$-118; (B) $CuO_x(1)/TiO_2$-38; and (C) $CuO_x(1)/TiO_2$-5.

458.5–458.9 eV. As regards the O 1s binding energy value, this is 530.3 eV for CuO and is about the same for the CuO_x/TiO_2 catalysts and the pure supports.

The Cu/Ti surface ratio determined by XPS is 0.11 for $CuO_x(\frac{1}{3})TiO_2$-38 and increases to 0.24 for $CuO_x(1)/TiO_2$-38. With further increase in CuO_x loading, however, the ratio remains almost constant. For freshly prepared $CuO_x(1)/TiO_2$-118 and $CuO_x(1)/TiO_2$-5 the Cu/Ti surface ratio is 0.14 and 0.22, respectively. After use in the incinerator of the $CuO_x(1)/TiO_2$ samples, the Cu/Ti surface ratio remains practically unchanged.

The intensity ratio between the Cu $2p_{3/2}$ shake-up satellite and the main peak is 0.53 for CuO and is slightly less for the supported copper oxide. This is due to photoreduction in the spectrometer of the dispersed copper oxide. Increase of the number of scans from one (Table 1) to eight generally caused a 50% decrease in the satellite to main peak ratio and a shift of the Cu $2p_{3/2}$ binding energy to about 932.7 eV. Such changes indicate reduction of Cu^{2+} to Cu^{1+} in agreement with a corresponding shift in the kinetic energy of the Cu $L_{2,3}M_{4,5}M_{4,5}$ Auger line (17).

FT-Raman Spectroscopy

The FT-Raman spectrum of the TiO_2-38 support and of prepared catalysts with different loading of CuO_x, together with the spectrum of pure CuO are shown in Fig. 10 for the region 200–1000 cm^{-1}. The TiO_2-38 support shows the characteristic spectrum of anatase (18) with four strong bands at 142, 396, 515, and 638 cm^{-1} and two weak bands at about 315 and 793 cm^{-1}. Pure CuO has one strong band at 296 cm^{-1} and two weak bands at 345 and 631 cm^{-1} in agreement with a previous report (19). The strongest band from CuO at 296 cm^{-1} grows with increased loading of CuO_x and can clearly be distinguished for the samples with 2.5 and 5.0 theoretical layers of CuO_x, but for $CuO_x(1)TiO_2$-38 the band is weak. In the case of $CuO_x(\frac{1}{3})/TiO_2$-38 only the bands from anatase are present. However, the intensity of the TiO_2 bands strongly decreases with increase in CuO_x loading. This shows again that the Raman technique is sensitive to the coverage of the support (20). Less than 10% of the intensity of the TiO_2-38 support bands remains in the spectrum for $CuO_x(\frac{1}{3})/TiO_2$-38 and there are no bands from CuO, indicating that the CuO_x species are well dispersed. With further increase in CuO_x loading, the intensity of the support bands, although less pronounced, continues to decrease, as shown in Fig. 11. This behavior indicates no further increase of the dispersion of copper oxide, but growth of CuO crystallites in agreement with the observed increase in intensity of the CuO band at 296 cm^{-1}.

The TiO_2-118 support showed only the characteristic anatase bands. After deposition of a theoretical monolayer of copper oxide, $CuO_x(1)/TiO_2$-118, a small band from CuO appeared at 296 cm^{-1}. Besides the anatase bands, the spectrum of the TiO_2-5 support showed a weak band at 445 cm^{-1} from rutile (18). Only the support bands were seen in the spectrum of the $CuO_x(1)/TiO_2$-5 sample, although compared with the TiO_2-5 spectrum, the bands were much less intense.

The used CuO_x/TiO_2 catalysts compared with the fresh catalysts showed no difference in Raman, except that the intensities of the anatase bands were generally slightly stronger in the spectra of the used catalysts.

TABLE 3

XPS Data Measured for the CuO_x/TiO_2 Catalysts and Supports

Sample	Cu $2p_{3/2}$ (eV)		Ti $2p_{3/2}$ (eV)		O 1s (eV)		Atomic ratio	Cu $2p_{3/2}$ ratio
	BE[a] (eV)	FWHM[b] (eV)	BE[a] (eV)	FWHM[b] (eV)	BE[a] (eV)	FWHM[b] (eV)	Cu/Ti	satellite/main peak
TiO_2-118	—	—	458.8	2.0	530.2	2.4	—	—
$CuO_x(1)/TiO_2$-118, fresh	934.3	4.2	458.9	2.4	530.4	2.8	0.14	0.48
$CuO_x(1)/TiO_2$-118, used[c]	934.2	3.8	458.6	2.5	530.0	2.8	0.13	0.45
TiO_2-38	—	—	458.8	2.0	530.0	2.5	—	—
$CuO_x(\frac{1}{3})/TiO_2$-38	934.4	4.6	458.9	2.4	530.2	2.8	0.11	0.43
$CuO_x(1)/TiO_2$-38, fresh	934.4	4.3	458.7	2.5	530.2	2.8	0.24	0.42
$CuO_x(1)/TiO_2$-38, used[c]	934.6	4.2	458.7	2.5	530.4	2.9	0.21	0.45
$CuO_x(2.5)/TiO_2$-38	934.2	4.2	458.7	2.4	530.1	2.7	0.21	0.41
$CuO_x(5)/TiO_2$-38	934.5	4.2	458.9	2.6	530.0	2.9	0.24	0.43
TiO_2-5	—	—	458.5	2.2	530.0	3.1	—	—
$CuO_x(1)/TiO_2$-5, fresh	934.6	4.3	458.6	2.4	530.2	3.1	0.22	0.49
$CuO_x(1)/TiO_2$-5, used[c]	934.7	4.1	458.8	2.4	530.2	3.1	0.25	0.50
CuO	934.3	3.8	—	—	530.3	3.4	—	0.53

[a] BE: binding energy.
[b] FWHM: full width at half maximum.
[c] After use for 57 days in the incinerator at a formaldehyde plant.

Scanning and Transmission Electron Microscopy

Scanning electron microscopy with EDX elemental mapping shows that the copper on $CuO_x(1)/TiO_2$-38 is evenly distributed throughout the pellet (Fig. 12). No difference between fresh and used sample was observed. Transmission electron microscopy with EDX analysis at higher resolution of the CuO_x/TiO_2-38 samples, with loadings from one-third of a monolayer up to five theoretical layers of CuO_x, shows the copper to be well dispersed for all the loadings. The TiO_2 crystallites do not change in size or shape with increased loading of CuO_x (Fig. 13), and high-resolution micrographs show no amorphous structure to be visible at the surfaces (Fig. 14). However, scarcely distributed CuO crystallites, roughly 60 nm in size, were found for $CuO_x(5)/TiO_2$-38, although the local variation in composition can be large (Fig. 15).

DISCUSSION

Base Metal Oxides on Titania

The results in Figs. 1 and 2 for CO and toluene combustion, respectively, over the various metal oxides on TiO_2 show that for CO the activity decreases in the order $CuO_x > CoO_x > MnO_x > FeO_x$. The stoichiometry cannot generally be given explicitly, because no XRD lines were observed from the active phase, indicating good dispersion or amorphous structure at this level of loading, i.e., a theoretical monolayer. For toluene combustion the corresponding order is $CuO_x > FeO_x > MnO_x > CoO_x$. Measurements of reaction rates using stoichiometric CO/O_2 mixtures have shown that at 227°C under steady state conditions, the specific activities of the unsupported oxides decrease in the following order: $Co_3O_4 > CuO_x > Mn_2O_3 > Fe_2O_3$ (21). For toluene oxidation at 400°C in air (air : toluene = 75 : 1), the results reported by Germain and Laugier (22) show the activity sequence as $Co_3O_4 > CuO > Mn_2O_3 \approx Fe_2O_3$. Our results for the supported oxides generally show the same activity sequences as those reported for the unsupported phases, but with two exceptions, namely (i) CuO_x is the most active structure on titania, and (ii) CoO_x on titania is not good for toluene combustion. The differences can be due to differing degrees of dispersion and active phase-support interaction. The high catalytic activity of CuO_x on titania is due to formation of dispersed copper oxide species, interacting with the titania surface. This conclusion agrees with the data in Fig. 4, showing that the activity remains almost constant when the CuO_x loading on TiO_2 is increased from one to five theoretical layers. Similar results for CO oxidation with the copper oxide content have been reported for coprecipitated Cu-Ce-oxide catalysts (23). Another example of spreading of active oxide on TiO_2 creating an active surface concerns the VO_x/TiO_2 system, which is active and selective for partial oxidation and ammoxidation of aromatics (24, 25).

Growth and Structure of Active CuO_x on TiO_2

Not only the activity measurements, but also the other characterisation methods reveal effective dispersion and spreading of CuO_x species on the TiO_2. XRD patterns for the CuO_x/TiO_2-38 samples show diffraction lines from bulk CuO only when the loading exceeds one theoretical monolayer (cf. Table 2). The corresponding Raman

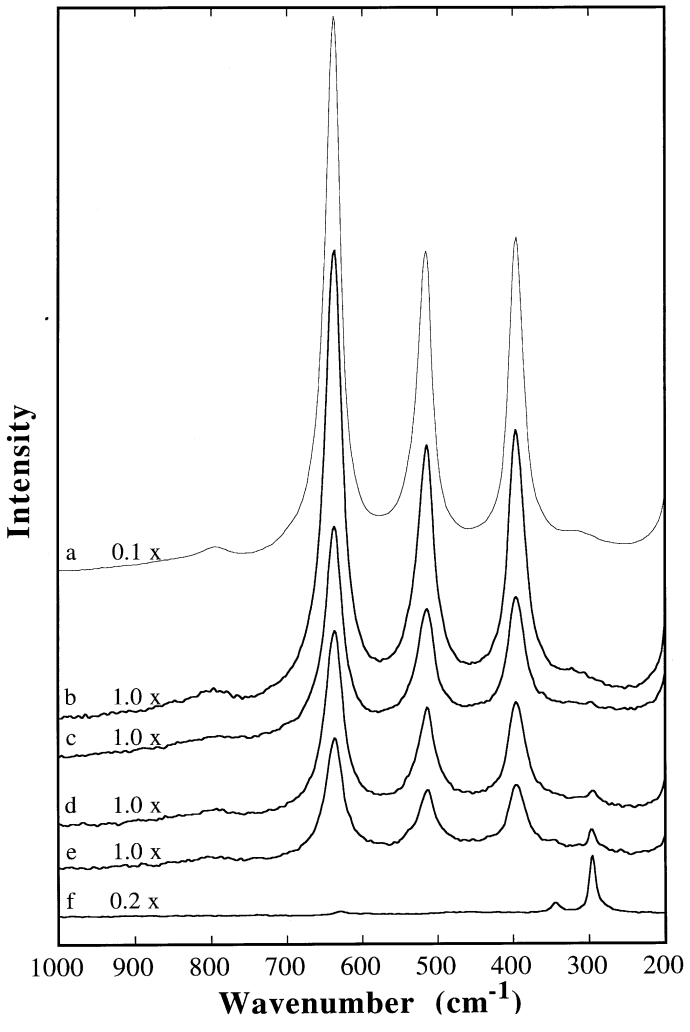

FIG. 10. FT-Raman spectra of (a) TiO_2-38; (b) $CuO_x(\frac{1}{3})/TiO_2$-38; (c) $CuO_x(1)/TiO_2$-38; (d) $CuO_x(2.5)/TiO_2$-38; (e) $CuO_x(5)/TiO_2$-38; and (f) CuO. Factors by which the Raman intensity has been multiplied are inserted.

spectra in Fig. 10 show formation of a small amount of bulk CuO for $CuO_x(1)/TiO_2$-38 as well, and the plot of the Raman intensity of the TiO_2 peak at 142 cm^{-1} against the CuO_x loading in Fig. 11 suggests formation of dispersed CuO_x species up to a loading in the range $\frac{1}{3}$–1 theoretical layer. EDX elemental maps (Fig. 12) and electron micrographs (Fig. 13) give additional support for the formation of dispersed CuO_x species. The reason for the micrographs in Fig. 13 of $CuO_x(1)/TiO_2$-38 and $CuO_x(5)/TiO_2$-38 being seemingly alike can be explained by formation of a few, scarcely distributed CuO crystals in the latter sample (Fig. 15). In agreement with previous microscopy results (11), however, resolving the dispersed CuO_x species on the titania surface was not possible. The XPS analyses of the variation of the Cu/Ti ratio with the loading (Table 3) also indicate effective dispersion of CuO_x at low loading. The Cu/Ti ratio increases up to a loading of one theoretical CuO_x layer and remains almost unchanged with further increase in loading.

TPR data, together with XPS results, give more details about the CuO_x structures on TiO_2. The TPR profiles in Fig. 8 show four peaks, which are at 180, 200, ≈250, and ≈400°C. The peak temperature is independent of the CuO_x loading, except for the peak at 250°C, for which the maximum shifts toward higher temperature with the increase in CuO_x loading. Several TPR results on titania supported copper oxide have been reported in the literature (11, 26–29). Some of these results concern supports containing the rutile polymorph of TiO_2. Considering the results previously reported for CuO_x on the anatase polymorph, the spectra in Fig. 8 show good agreement with those reported by Wöllner and co-workers (28) for similar calcination temperatures, showing reduction peaks at ≈190, 205, 270, and 420°C. Bond and co-workers (27) reported for CuO_x on Eurotitania (anatase) TPR maxima at about 140, 160, and 200°C. These temperatures are all 40°C below those obtained for the present samples. Considering that Bond *et al.* (27) reported the same type of intensity variations with increase in CuO_x loading as is shown in Fig. 8, it is most probable that the difference in temperature is due to experimental factors and, in fact, the

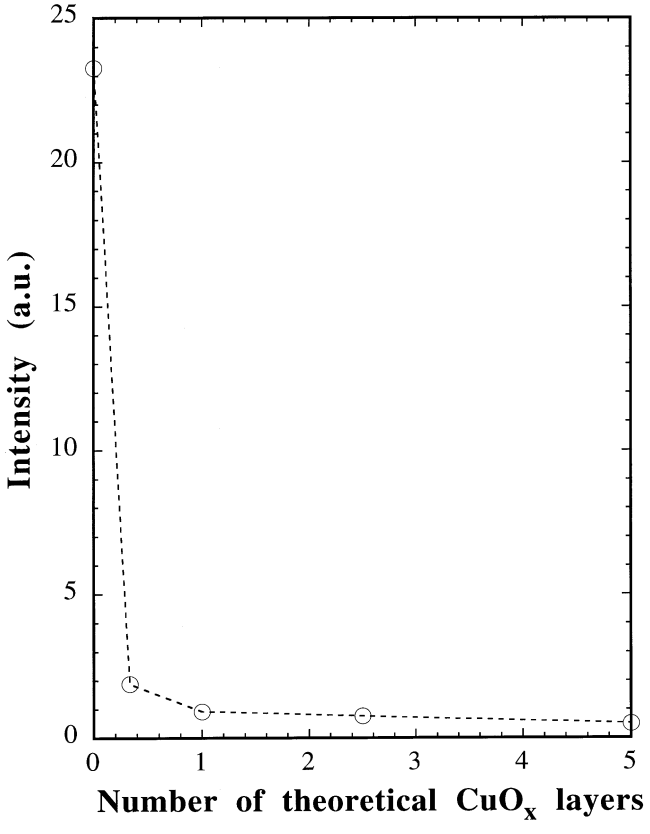

FIG. 11. Raman intensity of the TiO_2 anatase band at 142 cm^{-1} as a function the loading of CuO_x on TiO_2-38.

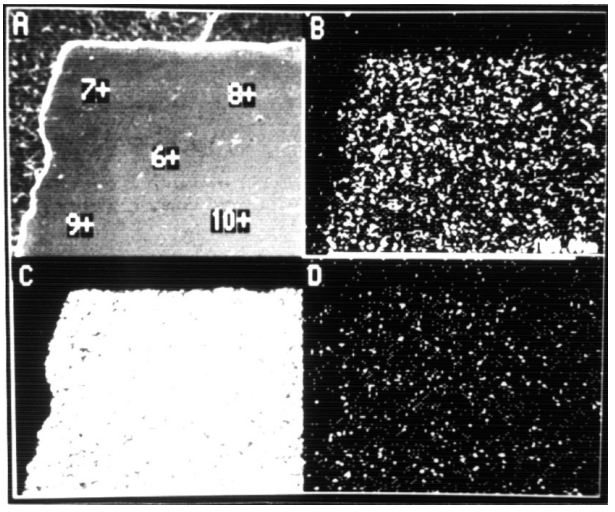

FIG. 12. EDX elemental maps for a cross section of a $CuO_x(1)/TiO_2$-38 pellet after being used for 57 days in an incinerator: (A) Secondary electron image. Spots for quantitative analyses are marked; (B) Cu-map; (C) Ti-map; and (D) map using background radiation next to characteristic peaks. An even distribution of Cu throughout the pellet can be observed (≈1 mm is shown).

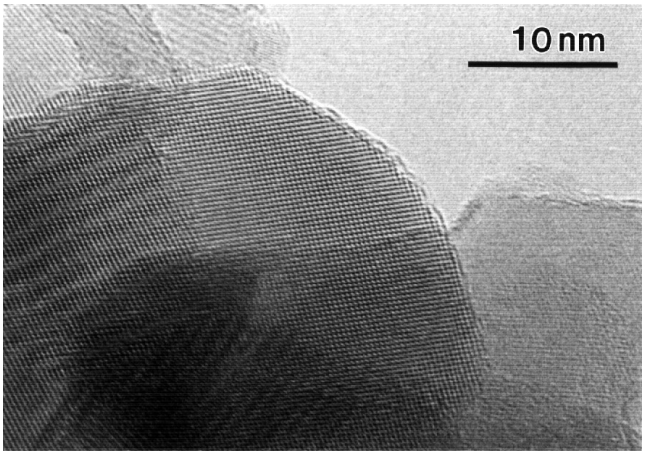

FIG. 14. High-resolution electron micrograph of $CuO_x(5)/TiO_2$-38. No amorphous structure is visible at the surface of the lattice-resolved crystal.

same types of CuO_x structures are formed on Eurotitania as on the present supports from Norton. The peak at 180°C possibly is from CuO_x species interacting with the titania surface, since the peak size remains almost constant with the increase in loading from one to five theoretical CuO_x layers. The peak at 200°C can be from another type of surface species, and the fact that in Fig. 8 the peak is most prominent in the profile of the sample with the lowest loading $CuO_x(\frac{1}{3})/TiO_2$-38 indicates that it can originate from an isolated dispersed species in contrast to the peak at 180°C, which can be from a polymeric CuO_x species. Formation of a polymeric monolayer or patches is in agreement with the finding that dispersed CuO_x species are formed up to a loading of almost one theoretical monolayer, corresponding to high coverage and a Cu/Ti interface ratio close to one.

The Cu $2p_{3/2}$, Ti $2p_{3/2}$, and O 1s binding energies in Table 3 of the samples agree well with published data for CuO (17, 28), CuO_x/TiO_2 samples (28) and TiO_2 (30). The XPS spectra of the catalysts show Cu $2p_{3/2}$ satellite/main peak ratios which are slightly less than the corresponding value for CuO. The difference is a consequence of the dispersed copper oxide species being more sensitive than bulk CuO to photoreduction in the spectrometer (see Experimental). Compounds with Cu^{1+} do not give any satellite, whereas there is one for Cu^{2+} compounds. For the latter the main peak has been related to a $2p^53d^{10}L$ final state, where L means a ligand hole, and the satellite peak to a $2p^53d^9$ final state (31). Usually Cu^{2+} compounds have Cu $2p_{3/2}$

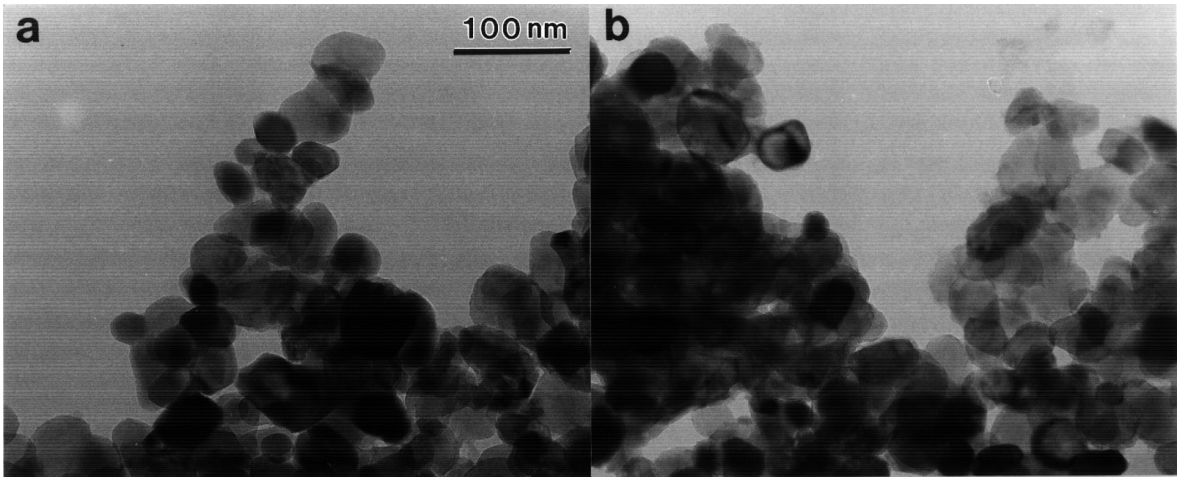

FIG. 13. Transmission electron micrographs of: (a) $CuO_x(1)/TiO_2$-38; and (b) $CuO_x(5)/TiO_2$-38. There is no apparent change with CuO_x loading in morphology or size of the TiO_2 support particles.

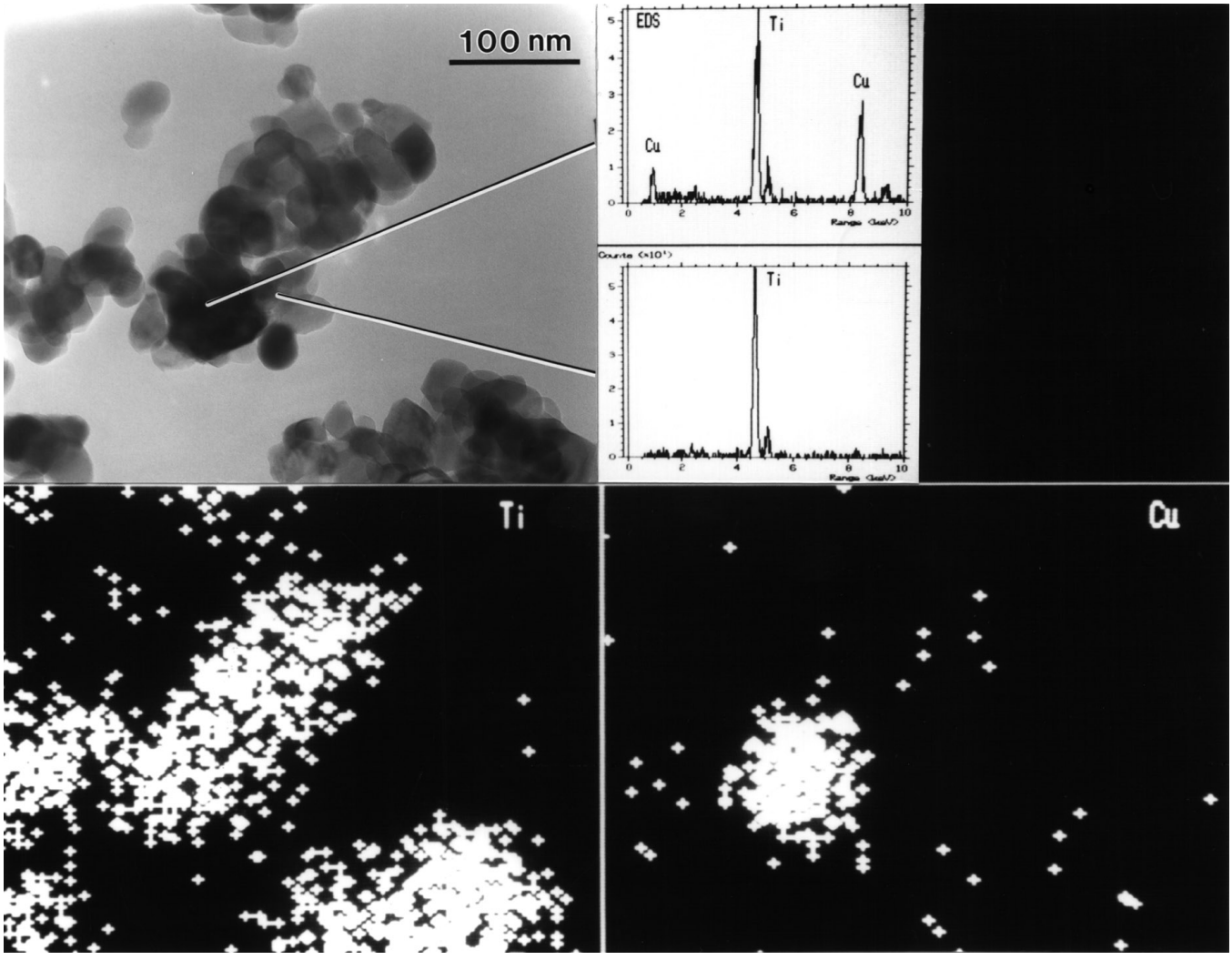

FIG. 15. TEM/STEM/EDX maps of $CuO_x(5)/TiO_2$-38. Crystalline Cu-rich particles, about 60 nm in size, localised by simultaneous Ti- and Cu-mapping, while eliminating average mass thickness effects by correlating with background maps.

satellite/main peak ratios which are in the range 0.3–0.9 (32). Thus, it can be concluded that the XPS data in Table 3 agree with the highly dispersed CuO_x species, interacting with the support, being Cu^{2+} centers. No direct proof was observed for the presence of Cu^{1+} species.

The Cu/Ti ratio determined by XPS does not change for CuO_x/TiO_2-38 when the CuO_x loading is increased above one theoretical layer, indicating growth of large CuO crystals. Formation of bulk CuO is shown by the XRD data in Table 2 and the Raman spectra in Fig. 10. Moreover, since the TPR peak at about 250°C (Fig. 8) grows progressively with increase in CuO_x loading, it can be assigned to the reduction of CuO not strongly interacting with the support. The TPR profiles in Figs. 9a and 9c for $CuO_x(1)/TiO_2$-118 and $CuO_x(1)/TiO_2$-5, respectively, show peaks from both dispersed species and CuO crystals. These catalysts, compared with $CuO_x(1)/TiO_2$-38 (Fig. 9b), have in fresh form comparatively more CuO particles (peak at 230–250°C. Likewise $CuO_x(1)/TiO_2$-38, the freshly prepared $CuO_x(1)/TiO_2$-5 sample shows the peak at ≈180°C, which was assigned to a polymeric CuO_x species of monolayer type. For the fresh $CuO_x(1)/TiO_2$-118, on the other hand, the low temperature peak is at 205°C and can be from an isolated CuO_x species, in accord with the assignment made for $CuO_x(\frac{1}{3})/TiO_2$-38.

Figures 8 and 9 show for the CuO_x/TiO_2-38 samples and $CuO_x(1)/TiO_2$-118 a TPR peak at about 400°C. This peak was absent in the spectra of the pure supports, which gave a peak around 650°C. It has been reported that the H_2 consumption during the reduction of CuO/TiO_2 considerably increases, compared with neat titania when the temperature is increased from 300°C to 500°C, and this was explained by the copper catalyzing reduction of the support (29). In their TPR experiments, Wöllner *et al.* (28) observed a hydrogen

consumption corresponding to a gross H_2/Cu ratio around 1.2 and suggested that the titania is reduced partially by H_2 dissociated on the reduced copper surface. Considering these results, the TPR peak at 400°C can be assigned to reduction of the titania surface caused by the spillover of hydrogen from the copper metal which is formed during the reduction process. The observation that the size of the peak is the same irrespective of the CuO_x loading on TiO_2-38 (cf. Fig. 8) is then due to the reduction of the titania surface being rate determining and not the dissociation of H_2. Figure 9c shows for $CuO_x(1)/TiO_2$-5 no peak at 400°C. A possible reason can be either stabilization of the titania due to the large particle size of this sample or the fact that the area of titania surface and interface per unit weight of sample is less than those of the other samples.

Calculation of the total amount of hydrogen which was consumed during the progress of the peaks for copper oxide at 180, 200, and ≈250°C did not give information about the valence of copper, since the molar ratio between the H_2 consumed and Cu was found to exceed unity by about 30%. Other investigators have reported the same finding (29), which can be due to some of the titania being reduced simultaneously with the copper oxide.

Our interpretation that on titania there are both dispersed CuO_x species, interacting with the titania, and CuO crystallites agrees with previous conclusions which were based on TPR (27) and diffuse reflectance data (33). In another work (28) the opinion was expressed that the various TPR peaks for copper oxide were from CuO particles of different sizes, because of the finding that the reduction profiles shifted toward higher temperatures when the calcination temperature was increased. Such interpretation of the present results disagrees with the TPR profiles in Fig. 8, showing that the low temperature peak is unaffected in size when the CuO_x loading goes from one to five theoretical layers. In contrast to a recent report (34), we found no evidence for the formation of an amorphous CuO layer on the titania (see Fig. 14).

Influence of Support Morphology

Comparison of the performances in Fig. 3 of monolayer CuO_x on the three titania supports shows that $CuO_x(1)/TiO_2$-38 is more active than $CuO_x(1)/TiO_2$-118, and $CuO_x(1)/TiO_2$-5 is the least active of the three catalysts for CO oxidation. The experiments were performed using a fixed volume of catalyst and, since the bulk density was approximately the same for the three catalysts, the ratios of surface areas loaded are directly proportional to the ratios of the specific surface areas (Table 1). Evidently, even though only 60% surface area, compared with $CuO_x(1)/TiO_2$-118, was loaded of $CuO_x(1)/TiO_2$-38, it is more active. The same relationship is true for toluene combustion (Fig. 6). Table 1 shows that the pores in $CuO_x(1)/TiO_2$-38 are generally larger than those in $CuO_x(1)/TiO_2$-118. Thus, the better performance of the former catalyst partly can be due to its having larger pores, making the diffusion of reactants and products easier. However, a good catalyst must have both enough surface area and pores which are not too small. A catalyst with large pores and consequently low specific surface area, or a nonporous material, will not be active in agreement with the results for $CuO_x(1)/TiO_2$-5. This catalyst, although it has the largest pores of the three samples (Table 1), including the macro-pores, is the least active per unit volume of catalyst (Fig. 3). A complication comparing the performances of copper oxide on the three supports is that the distribution between copper oxide species differs. $CuO_x(1)/TiO_2$-38 shows high coverage with polymeric CuO_x species, while $CuO_x(1)/TiO_2$-118 and $CuO_x(1)/TiO_2$-5 have crystalline CuO, together with isolated and polymeric CuO_x species, respectively. According to the TPR profiles of the latter two catalysts in Figs. 9a and 9c, at least half of the copper on these is in the form of bulk CuO. This implicates, compared with $CuO_x(1)/TiO_2$-38, lower coverage of the support with dispersed species interacting with the titania, a fact that contributes to their having lower activity.

The effect of pore size must be more evident at high temperature, since the rate constant of the surface reaction increases exponentially with increasing temperature. Therefore, the surface concentration of the limiting reactant will approach zero and the diffusion to the surface will become rate limiting (35). Although deactivation will be discussed in the following section, it is appropriate here to compare the pore sizes for the fresh and the used $CuO_x(1)/TiO_2$-38. The data is Table 1 show that the deactivation is accompanied by an increase of pore size. Comparison of the performances in CO oxidation is given in Fig. 7b for the fresh and the used catalyst, showing deactivation of the catalyst only at temperatures below 210°C and not at higher temperature where the conversion is high. The behavior illustrates the increasing importance of pore size with increase in temperature.

Catalyst Deactivation

Figure 7 shows deactivation of the $CuO_x(1)/TiO_2$ catalysts after being on stream for 57 days. $CuO_x(1)/TiO_2$-38, comparatively, shows the smallest deactivation among the three samples. The used $CuO_x(1)/TiO_2$-38 shows a temperature difference from the fresh sample of about 20°C, except at high temperatures, where the difference is much less due to the increase of the pore size upon usage (see the preceding section). The deactivation of samples is caused by sintering of both the support and the copper oxide. Sintering of the support is evident considering Table 1, which for $CuO_x(1)/TiO_2$-118 and $CuO_x(1)/TiO_2$-38 shows loss of surface area in agreement with the observed sharpening (see Table 2) of the corresponding XRD peaks after use of the samples. CuO_x/TiO_2-5 shows no loss of surface area

upon use, possibly because it consists of larger, more stable crystallites. Yuan *et al*. (26) and Amores *et al*. (36) have reported copper oxide induced sintering of TiO_2, which in part can explain the severe sintering of TiO_2-118 that is observed after deposition of copper and following calcination (Table 2).

Sintering of the copper oxide during use of the samples is apparent considering the TPR profiles in Fig. 9. Comparison of the recordings for the fresh with those for the used samples shows that the peaks from dispersed CuO_x species at 180 and ≈200°C have decreased in size, while there is a parallel growth of the peaks from crystalline CuO in the range 230–300°C. The XPS data in Table 3, however, show almost no change of the Cu/Ti ratios with use of the samples. For $CuO_x(1)/TiO_2$-118 and $CuO_x(1)/TiO_2$-38, showing sintering of the support, an unchanged Cu/Ti surface ratio is not in contrast with the TPR results. The new surfaces created as a result of the sintering can still be almost completely covered with dispersed species. The CuO crystallites, which form or grow in size simultaneously with sintering of the support, can become embedded among the support crystallites. Such an explanation does not hold for $CuO_x(1)/TiO_2$-5, which shows no sintering of the support upon use in the incinerator. However, for this sample great variation was noticed measuring the Cu/Ti ratio with XPS. This was possibly due to the difficulty, compared with $CuO_x(1)/TiO_2$-118 and $CuO_x(1)/TiO_2$-38, of collecting a representative sample because of its much larger crystallites.

The present results (Table 1 and Fig. 9) can thus explain the deactivation of the samples. $CuO_x(1)/TiO_2$-38 and $CuO_x(1)/TiO_2$-118 show sintering of both the support and the copper oxide. Although $CuO_x(1)/TiO_2$-38 shows the most severe sintering of the samples upon use in the incinerator, the deactivation of this sample is less pronounced. This observation can primarily be seen as due to the concurrent increase of the pore size giving better transport properties. The severe deactivation of $CuO_x(1)/TiO_2$-5 is a consequence of its low surface area and sintering of the active phase.

CONCLUSIONS

Copper oxide supported on titania shows good activity compared with cobalt, manganese, and iron oxides on the same support for the combustion of CO and toluene.

Characterisation with XRD, electron microscopy, EDX, Raman, TPR, and XPS reveals that the good performance of copper oxide on titania is due to spreading and formation of dispersed species on the surface. When the copper oxide loading is increased from one (12 μmol Cu/m^2) to five theoretical layers (60 μmol Cu/m^2) there is no further improvement in catalytic activity. This is due to formation of crystalline CuO particles, which contribute little to the active surface area. TPR profiles reveal the existence of two types of dispersed species interacting with the support, which possibly are isolated and polymeric (bidimensional) copper oxide, respectively. XPS data show that the dispersed species are Cu^{2+} species.

A good catalyst must have a suitable combination of surface area and pore size. A support from Norton, consisting of pure anatase with a surface area of 38 m^2/g and mainly meso-pores in the range 100–800 Å, is superior for use in a reactor of fixed volume to supports with either smaller surface area and macro-pores, or larger surface area and pores in the range 30–400 Å.

Deactivation of CuO_x/TiO_2 is occurring on treating the waste gas from a formaldehyde plant. After 57 days on stream, the inlet temperature has to be increased by ≈20°C to give the same conversion as a fresh catalyst. Sintering of both the support and the copper oxide causes the deactivation.

In comparison with a commercial metal oxide catalyst, CuO_x/TiO_2 shows better performance for CO and toluene combustion. A commercial Pt-based catalyst, however, is a better choice for toluene combustion, although for CO oxidation metal oxides can become alternative catalysts.

ACKNOWLEDGMENTS

Mrs. Birgitta Svensson is gratefully acknowledged for assisting with the BET and XRD analyses. Perstorp Formox is acknowledged for providing the facilities for activity measurements and deactivation studies, and we are grateful to the Norton Company for providing the titania supports. Financial support was received from the National Board for Industrial and Technical Development (NUTEK) and the Swedish National Research Council for Engineering Sciences (TFR).

REFERENCES

1. Noordally, E., Richmond, J. R., and Tahir, S. F., *Catal. Today* **17**, 359 (1993).
2. Wiederkehr, P., *in* "Characterization and Control of Odours and VOC in the Process Industries" (S. Vigneron, J. Hermia, and J. Chaouki, Eds.), Studies in Environmental Science, Vol. 61, p. 11. Elsevier, Amsterdam, 1990.
3. Bouscaren, R., Allemand, N., and Dang, Q. C., *in* "Characterization and Control of Odours and VOC in the Process Industries" (S. Vigneron, J. Hermia, and J. Chaouki, Eds.), Studies in Environmental Science, Vol. 61, p. 37. Elsevier, Amsterdam, 1990.
4. Moretti, E. C., and Mukhopadhyay, N., *Chem. Eng. Progress* **89**, 20 (1993).
5. Mazzarino, I., and Barresi, A. A., *Catal. Today* **17**, 335 (1993).
6. Ruddy, E. N., and Carroll, L. A., *Chem. Eng. Progress* **89**, 28 (1993).
7. Freidel, I. M., Frost, A. C., Herbert, K. J., Meyer, F. J., and Summers, J. C., *Catal. Today* **17**, 367 (1993).
8. Prasad, R., Kennedy, L. A., and Ruckenstein, E., *Combust. Sci. Technol.* **22**, 271 (1980).
9. Davydova, L. P., Popovskii, V. V., Bulgakov, N. N., Davydov, A. A., Kazakova, A. A., and Dobrynkin, N. M., *Kinet. Katal.* **29**, 1162 (1988).
10. Satterfield, C. N., "Heterogeneous Catalysis in Industrial Practice," 2nd ed., p. 123. McGraw–Hill, New York, 1991.
11. del Arco, M., Caballero, A., Malet, P., and Rives, V., *J. Catal.* **113**, 120 (1988).

12. Sanati, M., and Andersson, A., *J. Mol. Catal.* **59**, 233 (1990).
13. JCPDS International Centre for Diffraction Data, "Powder Diffraction File," Swarthmore, PA, 1991.
14. Barrett, E. P., Joyner, L. G., and Halenda, P. H., *J. Am. Chem. Soc.* **73**, 373 (1951).
15. Froment, G. F., and Bischoff, K. B., "Chemical Reactor Analysis and Design," 2nd ed., Wiley, New York, 1990.
16. Spurr, R. A., and Myers, H., *Anal. Chem.* **29**, 760 (1957).
17. Otamiri, J. C., Andersson, S. L. T., and Andersson, A., *Appl. Catal.* **65**, 159 (1990).
18. Schraml-Marth, M., Wokaun, A., and Baiker, A., *Fresenius J. Anal. Chem.* **341**, 87 (1991).
19. Reimann, K., and Syassen, K., *Solid State Commun.* **76**, 137 (1990).
20. Sanati, M., Andersson, A., Wallenberg, L. R., and Rebenstorf, B., *Appl. Catal. A* **106**, 51 (1993).
21. Boreskov, G. K., *in* "Catalysis—Science and Technology" (J. R. Anderson and M. Boudart, Eds.), Vol. 3, p. 39. Springer-Verlag, Berlin, 1982.
22. Germain, J.-E., and Laugier, R., *Bull. Soc. Chim. France*, 541 (1972).
23. Liu, W., and Flytzani-Stephanopoulos, M., *J. Catal.* **153**, 304 (1995).
24. Gasior, M., Haber, J., and Machej, T., *Appl. Catal.* **31**, 1 (1987).
25. Sanati, M., Wallenberg, L. R., Andersson, A., Jansen, S., and Tu, Y., *J. Catal.* **132**, 128 (1991).
26. Yuan, S., Mériaudeau, P., and Perrichon, V., *Appl. Catal. B* **3**, 319 (1994).
27. Bond, G. C., Namijo, S. N., and Wakeman, J. S., *J. Mol. Catal.* **64**, 305 (1991).
28. Wöllner, A., Lange, F., Schmelz, H., and Knözinger, H., *Appl. Catal. A* **94**, 181 (1993).
29. Delk II, F. S., and Vävere, A., *J. Catal.* **85**, 380 (1984).
30. Nogier, J. Ph., and Delamar, M., *Catal. Today* **20**, 109 (1994).
31. van der Laan, G., Westra, C., Haas, C., and Sawatzky, G. A., *Phys. Rev. B* **23**, 4369 (1981).
32. Frost, D. C., Ishitani, A., and McDowell, C. A., *Mol. Phys.* **24**, 861 (1972).
33. Talipova, Sh. A., and Vorobiev, V. N., *React. Kinet. Catal. Lett.* **32**, 469 (1986).
34. Boccuzzi, F., Guglielminotti, E., Martra, G., and Cerrato, G., *J. Catal.* **146**, 449 (1994).
35. Prasad, R., Kennedy, L. A., and Ruckenstein, E., *Catal. Rev. Sci. Eng.* **26**, 1 (1984).
36. Amores, J. M. G., Escribano, V. S., Busca, G., and Lorenzelli, V., *J. Mater. Chem.* **4**, 965 (1994).